# *Studies on new hybrid materials prepared by both Diels–Alder and Michael addition reactions*

## Cristian-Dragos Varganici, Oana Ursache, Constantin Gaina, Viorica Gaina & Bogdan C. Simionescu

**Journal of Thermal Analysis and Calorimetry**
An International Forum for Thermal Studies

ISSN 1388-6150
Volume 111
Number 2

J Therm Anal Calorim (2013)
111:1561-1570
DOI 10.1007/s10973-012-2532-y

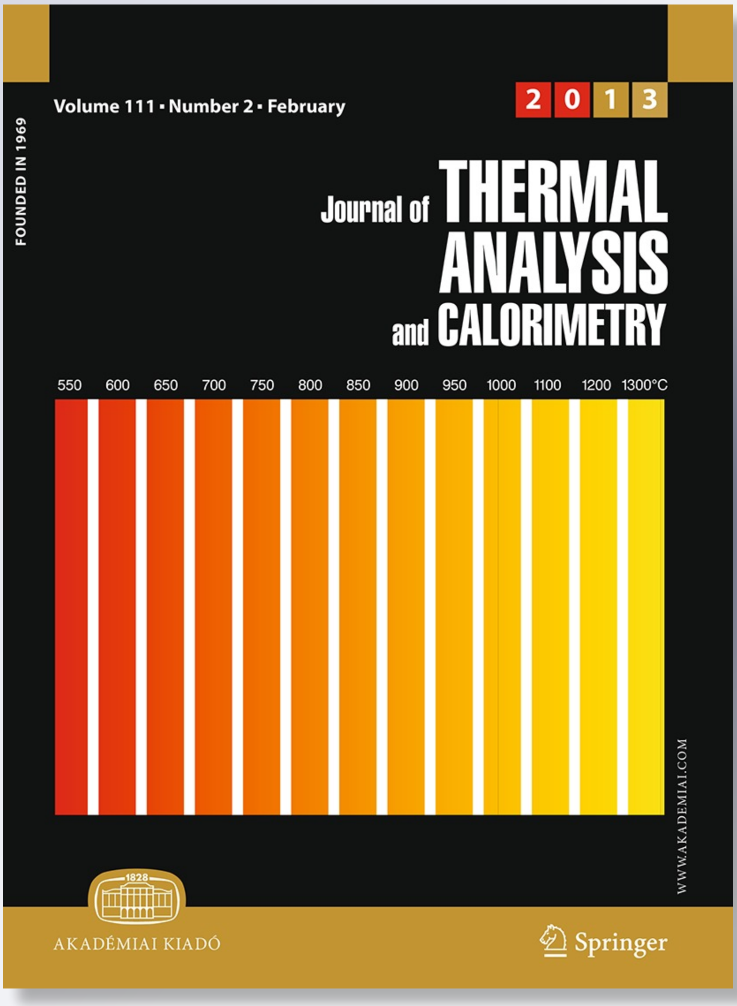

J Therm Anal Calorim (2013) 111:1561–1570
DOI 10.1007/s10973-012-2532-y

# Studies on new hybrid materials prepared by both Diels–Alder and Michael addition reactions

**Cristian-Dragos Varganici · Oana Ursache ·
Constantin Gaina · Viorica Gaina ·
Bogdan C. Simionescu**

Received: 16 January 2012 / Accepted: 4 June 2012 / Published online: 4 July 2012

**Abstract** New polyurethane chemically crosslinked networks containing silica were synthesized by both Diels–Alder polymerization and Michael addition reaction. Structural characterization of the products was evidenced by proton nuclear magnetic resonance and attenuated total reflectance in conjunction with Fourier transform infrared spectroscopy techniques. Differential scanning calorimetry was used to demonstrate the thermally remendable character of the materials obtained through Diels–Alder polymerization. The influence of increasing silica content on the glass transition temperatures was studied. It was observed that the glass transition temperatures increased with increasing silica content. Absolute heat capacities and crosslinking densities were determined for the thermoreversible materials. A comparison between materials obtained through Diels–Alder process and Michael addition method was studied. A kinetic study was conducted via an isoconversional method. Morphological studies were conducted by atomic force microscopy technique.

**Keywords** Hybrid materials · Retro-Diels–Alder · Michael addition · Thermal remendability

## Introduction

The quantitative recovery of polymers and their corresponding monomers from polymer-containing waste has become a real worldwide challenge in conserving petroleum resources, even for the most easily recyclable materials. In order to overcome this aspect, the research domains in obtaining polymeric materials which combine easy recycling, utilization of renewable resources, mild synthetic reaction conditions, and biodegradability are constantly expanding [1]. For these purposes, smart polymers [2–6] or materials which can respond to several different external stimuli, such as change of temperature, pH, atmosphere, light, magnetic field, and electric field, needed to be synthesized. The properties of these polymers permit them to be used in self-healing materials, in biomaterials for biomedical applications, in microelectronic applications, and in materials with memory shape capacity [2–5].

Chemical recycling processes have proven to be more and more effective. They consist in the depolymerization and repolymerization cycles of the comprising monomers with the reproduction of the initial polymeric material [7, 8]. However, limitations in obtaining crosslinked structures with such properties exist due to the use of traditionally covalent reactions in the crosslinking step with the result of irreversible networks. Because of this aspect, such networks exhibit severe limitations, e.g., lack of control over the structural design of the final network and potential side reactions (e.g., chain degradation) leading to limited processing ability and remendability. In order to surpass this impediment, the possibilities for reversible

---

C.-D. Varganici (✉) · B. C. Simionescu (✉)
Centre of Advanced Research in Bionanoconjugates and Biopolymers, "Petru Poni" Institute of Macromolecular Chemistry, 41A Gigore Ghica-Voda Alley,
700487 Iasi, Romania
e-mail: varganici.cristian@icmpp.ro

B. C. Simionescu
e-mail: bcsimion@icmpp.ro

O. Ursache · C. Gaina · V. Gaina · B. C. Simionescu
"Petru Poni" Institute of Macromolecular Chemistry,
41A Grigore Ghica-Voda Alley, 700487 Iasi, Romania

B. C. Simionescu
Department of Natural and Synthetic Polymers, "Gh. Asachi" Technical University of Iasi, 73 B-dul Dimitrie Mangeron,
700050 Iasi, Romania

crosslinking reactions were exploited, including the obtaining of thermoreversible crosslinked networks containing Diels–Alder (DA) adducts [9–12]. However, literature in this research area is only limited to the preparation of polymers or monomers containing a furan derivative which reacts with a dienophile [13–19]. The three most important advantages of the DA reaction are the following: both DA and retro-Diels–Alder (rDA) reactions proceed under relatively mild conditions, require no additives such as catalyst, and generate no by-products.

In this paper, authors report the synthesis of new hybrid networks containing polyurethanic chains and silica via DA and Michael addition (MA) reaction and characterize them by proton nuclear magnetic resonance ($^1$H-NMR), attenuated total reflectance in conjunction with Fourier transform infrared spectroscopy (ATR–FTIR), differential scanning calorimetry (DSC), and atomic force microscopy (AFM) methods.

## Materials and methods

### Materials

(3-Aminopropyl)triethoxysilane (APTEOS) (Fluka), 3-isocyanatopropyltriethoxysilane (IPTEOS) (Aldrich), tetraethyl orthosilicate (TEOS) (Fluka), dibutyltin dilaureate (DBTDL) (Merck-Schuchardt), 2-furfuryl alcohol (Aldrich), dimethylformamide (DMF) (Aldrich), tetrahydrofuran (THF) (Aldrich), acetonitrile (Aldrich) were used as received. Bismaleimide containing urethane groups (BMI) was prepared by a method described in a previous paper [20]. 2-Furylmethyl-(propyltriethoxysilane) carbamate (FPTEOS) was synthesized by a method described below.

### Synthesis

#### *2-Furylmethyl-(propyltriethoxysilane) carbamate*

2-Furylmethyl-(propyltriethoxysilane) carbamate (FPTEOS) was synthesized by addition reaction of 2-furfuryl alcohol to IPTEOS in THF in the presence of DBTDL as catalyst. After removing the solvent, a yellow viscous product was obtained; FTIR (KBr, cm$^{-1}$): 3340, 2975, 2928, 2886, 1724, 1533, 1443, 1390, 1245, 1165, 1103, 1079, 957 and 777; $^1$H-NMR (CDCl$_3$-TMS), $\delta$ (ppm): 7.40 (s, 1H, 5-furyl proton), 6.38 (d, 1H, $J = 2.3$ Hz, 3-furyl proton), 6.345 (dd, 1H, $J_1 = 2$, $J_2 = 3.2$ Hz, 4-furyl proton), 5.3 (m, 1H, N$\underline{H}$), 5.1 (s, 2H, C$\underline{H}_2$-furyl), 3.8 (m, 6H, C$\underline{H}_2$–O), 3.15 (m, 2H, C$\underline{H}_2$–NH), 1.62 (m, 2H, C$\underline{H}_2$), 1.23 (t, 9H, C$\underline{H}_3$), 0.64 (m, 2H, C$\underline{H}_2$–Si).

#### *Bis(triethoxysilane) monomers by DA cycloaddition*

To a solution of urethane-bismaleimide (BMI) (1.0 mmol) in acetonitrile (10 mL), FPTEOS was added (2.0 mmol) and stirred at 80 °C for 12 h. After recovering the solvent a yellow wax was obtained; FTIR (KBr, cm$^{-1}$): 3990, 2938, 2852, 1776, 1710, 1605, 1542, 1516, 1393, 1315, 1230, 1108, 1075, 839, 772, 688; $^1$H-NMR (CDCl$_3$-TMS), $\delta$ (ppm): 7.46 (d, 4H, aromatic protons), 7.17 (d, 4H, aromatic protons), 7.05 (m, 2H, N$\underline{H}$-phenyl), 6.55 (d, 4H, HC=CH cycloadduct protons), 5.37 (m, 4H, 2 protons of C$\underline{H}_2$–NH–COO and 2 protons of C$\underline{H}$–O cycloadduct), 5.04 (m, 4H, C$\underline{H}_2$-furyl), 4.18 (m, 4H, C$\underline{H}_2$–COO), 3.80 (m, 12H, C$\underline{H}_2$–O–Si), 3.64 (m, 2H, CH of succinimide cycloadduct), 3.42 (m, 32H, C$\underline{H}_2$–O from poly(tetrahydrofuran) (PTHF) structure), 3.17 (m, 4H, C$\underline{H}_2$–NH), 3.11 (m, 2H, CH of succinimide cycloadduct), 1.62 (m, 40H, 36 protons CH$_2$ from PTHF structure and 4H of C$\underline{H}_2$–CH$_2$–Si), 1.21 (t, 18H, C$\underline{H}_3$), 0.61 (m, 4H, C$\underline{H}_2$–Si).

#### *Bis(triethoxysilane) monomers by MA reaction*

To a solution of BMI (1.0 mmol) in THF (10 mL), APTEOS (2.0 mmol) was added and stirred at room temperature for 24 h. After removing the solvent a yellow wax was obtained; FTIR (KBr, cm$^{-1}$): 3440, 2927, 2852, 1719, 1612, 1538, 1517, 1404, 1313, 1224, 1114, 1065, 835, 684; $^1$H-NMR (CDCl$_3$-TMS), $\delta$ (ppm): 7.48 (d, 4H, aromatic protons), 7.18 (d, 4H, aromatic protons), 7.08 (m, 2H, N$\underline{H}$), 6.73 (m, 2H, N$\underline{H}$), 4.18 (t, 4H, C$\underline{H}_2$–OOC), 3.85 (m, 2H, C$\underline{H}$ of succinimide ring), 3.81 (m, 12H, C$\underline{H}_2$–O–Si), 3.42 (m, 32H, C$\underline{H}_2$–O from PTHF), 3.06 (dd, 2H, C$\underline{H}$ of succinimide ring), 2.84 (m, 4H, C$\underline{H}_2$–NH), 2.37 (dd, 2H, succinimide ring) 1.73 (m, 4H, C$\underline{H}_2$–CH$_2$–Si), 1.63 (m, 36H, CH$_2$ protons from PTHF structure), 1.22 (t, 18H, C$\underline{H}_3$), 0.68 (m, 4H, C$\underline{H}_2$–Si).

#### *Synthesis of polyurethane networks based on DA monomers (PUSHDAN)*

To a solution of BMI (0.001 mol, 1.08 g) in DMF (15 mL), FPTEOS (0.002 mol, 0.69 g) was added and stirred at 80 °C for 8 h. The solution was cooled at room temperature and mixed with pre-established amounts of TEOS according to Table 1. After about 5 min of stirring, 3 drops of DBTDL and 3 drops of water were added and the stirring continued for 10 min at room temperature and 2 h at 60 °C. The resulted mixture was used to obtain films by pouring on a Teflon foil. The films were maintained at 80 °C for 48 h and another 12 h in vacuum at 80 °C. The obtained colourless and transparent films (with a 0.1–0.25 mm thickness) were easily peeled off from the substrate.

**Table 1** Composition of hybrid materials

| Network | BMI/g | FPTEOS/g | APTEOS/g | TEOS/g | Silicate content*/% |
|---|---|---|---|---|---|
| PUSHDAN-1 | 1.08 | 0.65 | – | – | 8.28 |
| PUSHDAN-2 | 1.08 | 0.65 | – | 1 | 21.47 |
| PUSHDAN-3 | 1.08 | 0.65 | – | 2 | 29.15 |
| PUSHMAN-1 | 1.08 | – | 0.44 | – | 10.05 |
| PUSHMAN-2 | 1.08 | – | 0.44 | 1 | 27.61 |
| PUSHMAN-3 | 1.08 | – | 0.44 | 2 | 35.31 |

* As calculated from the added quantity of FPTEOS, APTEOS or TEOS

### *Synthesis of polyurethane networks by Michael addition (PUSHMAN)*

To a solution of BMI (0.001 mol, 1.08 g) in DMF (15 mL), APTEOS (0.002 mol, 0.47 mL) was added. The solution was stirred at room temperature for 6 h and mixed with pre-established amounts of TEOS according to Table 1. Further, the same procedure as in the case of PUSHDAN was followed.

## Measurements

### *ATR–FTIR*

The FTIR spectra were recorded on a Bruker Vertex 70 Instrument equipped with a Golden Gate single reflection ATR accessory, spectrum range 600–4,000 cm$^{-1}$.

### *$^{1}$H-NMR*

The $^{1}$H-NMR spectra were recorded on a Bruker NMR spectrometer, Avance DRX 400 MHz, using DMSO-d$_6$ as solvents and tetramethylsilane as an internal standard.

### *DSC*

DSC measurements were conducted on a DSC 200 F3 Maia (Netzsch, Germany). A mass of 10 mg of each sample was heated in pressed and pierced aluminum crucibles at a heating rate of 20 °C min$^{-1}$. Nitrogen was used as inert atmosphere at a flow rate of 50 mL min$^{-1}$. The temperature against heat flow was recorded. The baseline was obtained by scanning the temperature domain of the experiments with an empty pan. The enthalpy was calibrated with an indium standard as well as the heat capacity was calibrated by measuring with sapphire disk supplied by Netzsch.

### *Crosslinking densities determination*

Crosslinking densities were calculated following the method described by Vera-Graziano et al. [21], using Eq. (1):

$$\rho'_{\mathrm{c}} = \frac{C_{\mathrm{p}}^{i} - C_{\mathrm{p}}^{0}}{C_{\mathrm{p}}^{0}} = \frac{\Delta C_{\mathrm{p}}^{i}}{C_{\mathrm{p}}^{0}} \tag{1}$$

where $C_{\mathrm{p}}^{i}$ and $C_{\mathrm{p}}^{0}$ are the heat capacities of the polymer network at a given crosslinking density, $(\rho'_{\mathrm{c}})^{i}$, and that of macromonomer BTESDAM, respectively. In order to determine the heat capacities, several heating curves were measured in the temperature range from 30 to 180 °C all at the same heating rate of 20 °C min$^{-1}$. First, a baseline for the DSC cell, *B*, was recorded using two aluminum empty crucibles as sample and reference, respectively. After that, a heating curve was recorded for a reference sample, *R*, consisting of pure sapphire. This procedure was repeated before recording every heating curve, *S*, for each sample in Fig. 5. The difference in heat flow signal between the sample and baseline and the total area between the curves was measured. Then, the absolute heat capacities ($C_{\mathrm{p}}s$) of the samples at given temperatures were obtained by the height differences relation, using Eqs. (2) and (3):

$$C_{\mathrm{p}}(\mathrm{sample}) = \frac{S - B}{R - B} \tag{2}$$

$$C_{\mathrm{p}}(\mathrm{sample}) = \frac{m_{\mathrm{sapphire}} \cdot D_{\mathrm{p}}(\mathrm{sample})}{m_{\mathrm{sample}} \cdot D_{\mathrm{p}}(\mathrm{sapphire})} \cdot C_{\mathrm{p}}(\mathrm{sapphire}) \tag{3}$$

where $D_{\mathrm{p}}$(sapphire) and $D_{\mathrm{p}}$(sample) are the effective displacements of sapphire and sample, respectively; $m_{\mathrm{sapphire}}$ and $m_{\mathrm{sample}}$ are the masses of sapphire and sample, in mg, respectively; and $C_{\mathrm{p}}$(sapphire) is the absolute heat capacity of sapphire (in J g$^{-1}$ K$^{-1}$) from the literature [22]. Such determinations were made by instantaneously raising the sample temperature one degree (from $T_{\mathrm{x}}$ to $T_{\mathrm{x+1}}$). The area limited by the curve and the baseline, between $T_{\mathrm{x}}$ and $T_{\mathrm{x+1}}$, is the heat capacity, in accordance with its definition [23, 24]. Determinations were properly done because of the

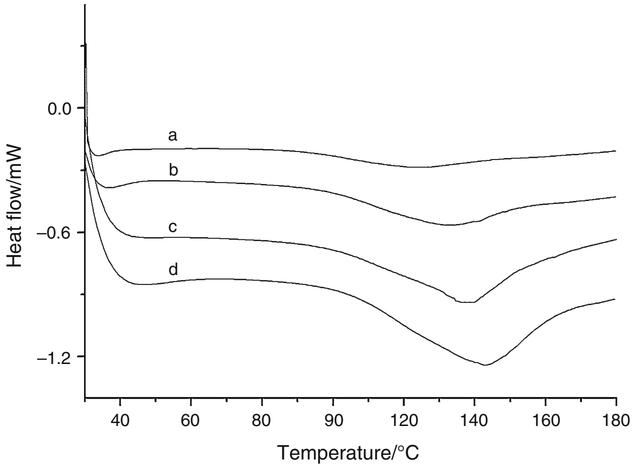

**Fig. 1** DSC heating curves: *a* 5 °C $\min^{-1}$, *b* 10 °C $\min^{-1}$, *c* 15 °C $\min^{-1}$ and *d* 20 °C $\min^{-1}$

small thermal inertia of the DSC equipment allowing the sample to absorb only the required energy to raise its temperature just one degree in the elapsed time.

### *Kinetic parameters determination*

Global kinetic parameters of the rDA reaction were determined by Flynn–Wall–Ozawa method (FWO) [26–30] which uses shifts in the temperature domain of the heating curves with heating rate increase. For this purpose, approximately the same mass (10 mg) of a sample obtained through DA reaction (PUSHDAN-3) was heated at four different heating rates of 5, 10, 15, and 20 °C $\min^{-1}$, respectively (Fig. 1). The values of the peak temperatures ($T_p$) and of the enthalpies of the endothermic process at all four heating rates are given in Table 2. The final form of the mathematical expression of FWO method by Doyle approximation [25, 31], is given in Eq. (4):

$$\frac{d(\log\beta)}{d(1/T_p)} = -\frac{0.4567E_a}{R} \tag{4}$$

where $E_a$ is the activation energy (kJ $\mathrm{mol}^{-1}$), $\beta$ is the heating rate (°C $\min^{-1}$), and $R$ is the gas constant (8.314 J $\mathrm{mol}^{-1}$ $\mathrm{K}^{-1}$).

If the assumption of a first order reaction proves valid, for the same value of $\alpha$, the plot of $\log\beta$ as a function of $1/T_p$ is a straight line with the slope proportional with the $E_a$. The pre-exponential factor $A$ ($\mathrm{s}^{-1}$) can be determined using Eq. (5) [32]:

$$A = \frac{\beta \times E_a \times \exp(E_a/R \times T_p)}{R \times T_p^2} \tag{5}$$

The non-isothermal heating curves were processed by means of Netzsch Thermokinetics 3 software.

**Table 2** Peak temperatures and enthalpy values of endothermal reaction (°C)

| Heating rate, $v_h$/°C $\min^{-1}$ | $T_p$/°C | $\Delta H$/J $\mathrm{g}^{-1}$ |
|---|---|---|
| 5 | 124.17 | −42.51 |
| 10 | 133.03 | −39.18 |
| 15 | 137.75 | −43.84 |
| 20 | 143.04 | −39.07 |

### *AFM*

AFM images were collected in semicontact mode using a Solver PRO-M, NT-MDT, Russia.

## Results and discussion

### Synthesis

The polyurethane silica containing crosslinked networks were synthesized by both DA and MA reactions of BMI using FPTEOS or APTEOS, respectively, followed by sol–gel process of triethoxysilane groups and TEOS (Scheme 1; Table 1).

The ATR–FTIR spectra confirmed the proposed structures. The reaction between BMI and FPTEOS was monitored by the disappearance of the characteristic peak of maleimide group at 1,158 $\mathrm{cm}^{-1}$ and the decrease of the overlapping band NH–COO (urethane) and C=C (in furan) at 1,535 $\mathrm{cm}^{-1}$ (Fig. 2). There, two new absorption bands which appeared at 1,776 $\mathrm{cm}^{-1}$ due to the maleimide-furan cycloadduct [33] and at 1,195 $\mathrm{cm}^{-1}$ due to asymmetric $\nu_{\mathrm{C-N-C}}$ of cycloadduct and a decrease in intensity of the bands at 1704, 834 and 689 $\mathrm{cm}^{-1}$ attributed to the maleimide group can also be observed. After the sol–gel process takes place, a new absorption band appears in the spectra of PUSHDAN-1-3 at 1,069 $\mathrm{cm}^{-1}$ attributed to the asymmetric stretching of the Si–O–Si group [34]. The intensity of this band increases from PUSHDAN-1 to PUSHDAN-3 due to the increase of the Si–O–Si groups in the hybrid network with increasing TEOS content. As it can be observed, in the ATR–FTIR spectra of the hybrid materials obtained by Michael addition reaction, PUSHMAN-(1-3), there are no major differences comparing with the spectra of PUSHDAN-(1-3). However, it should be noted that the symmetric and asymmetric absorption bands characteristic to the carbonyl group are shifted to higher wavenumbers in the case of the Michael addition products.

### Thermally reversible polyurethane networks

The DA and rDA reactions of hybrid polyurethane networks were monitored by ATR–FTIR spectroscopy and DSC measurements.

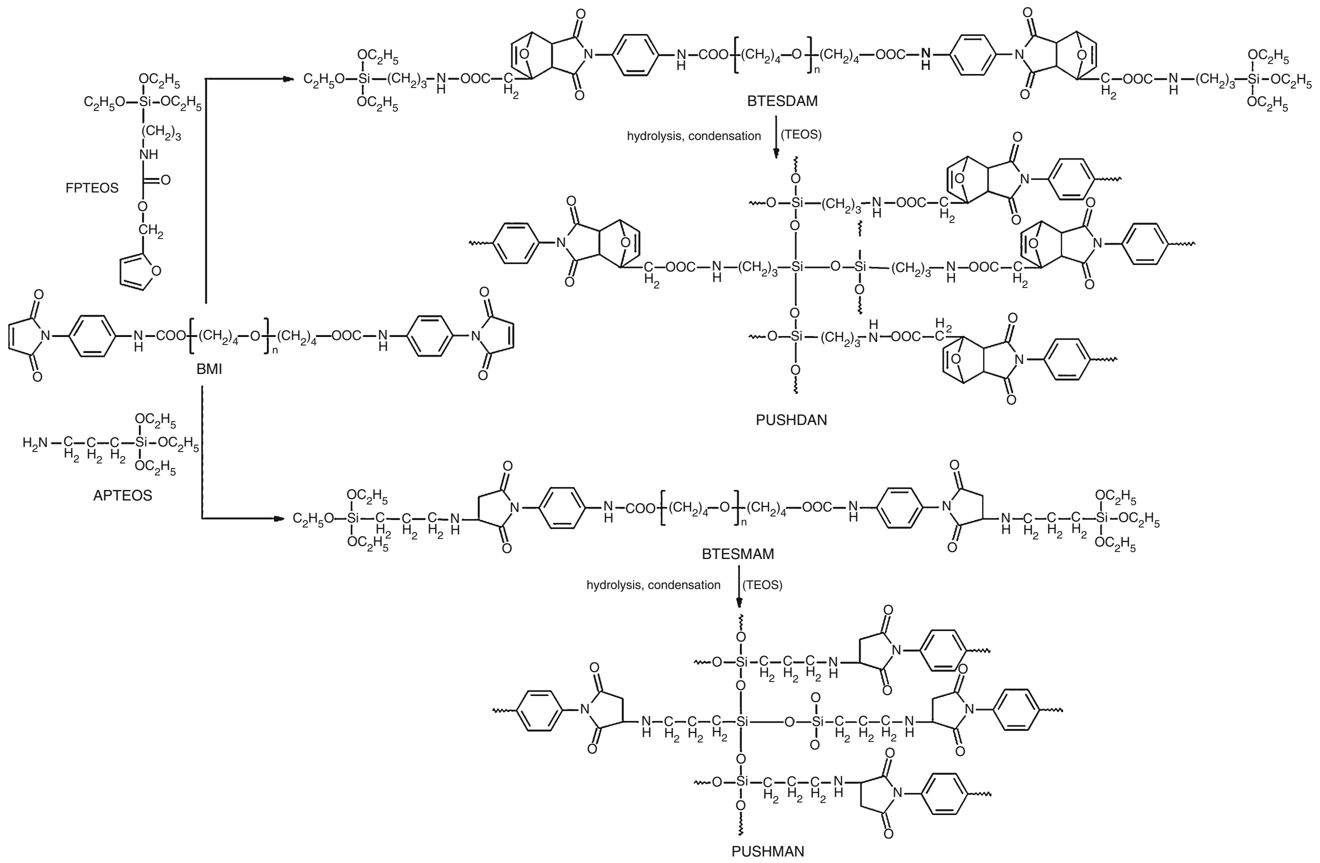

**Scheme 1** Synthesis of the crosslinked hybrid networks

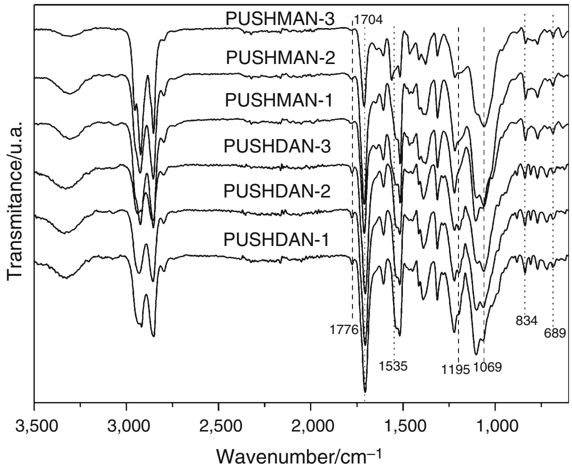

**Fig. 2** ATR–FTIR spectra of the hybrid materials

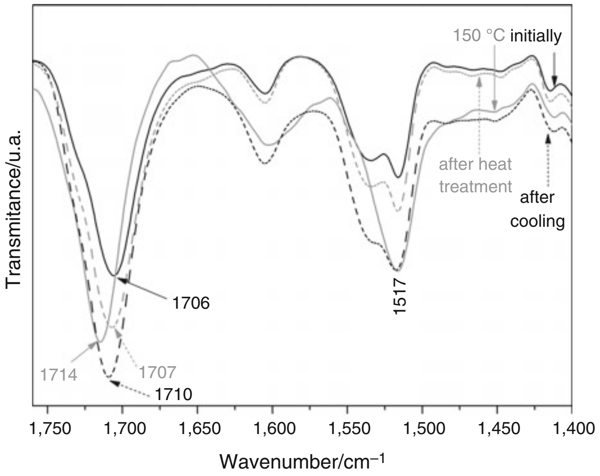

**Fig. 3** ATR–FTIR spectra of sample PUSHDAN-2

### *ATR–FTIR*

The ATR–FTIR spectra of PUSHDAN-2 films recorded at 25, 150 °C, after cooling at 25 °C, and after curing the sample at 80 °C for 6 h are presented in Fig. 3. By heating PUSHDAN-2 at 150 °C, the furan-maleimide cycloadducts from the crosslinked network de-bonded generating free furan groups which resulted in an increase of the absorption band at 1,518 cm$^{-1}$ (spectrum b). Also, the retrodienic process is indicated by the fact that the carbonyl absorption band shifts to higher wavenumber (from 1,706 to 1,714 cm$^{-1}$). The de-bonded crosslinking sites have partially formed again when cooling the sample. The

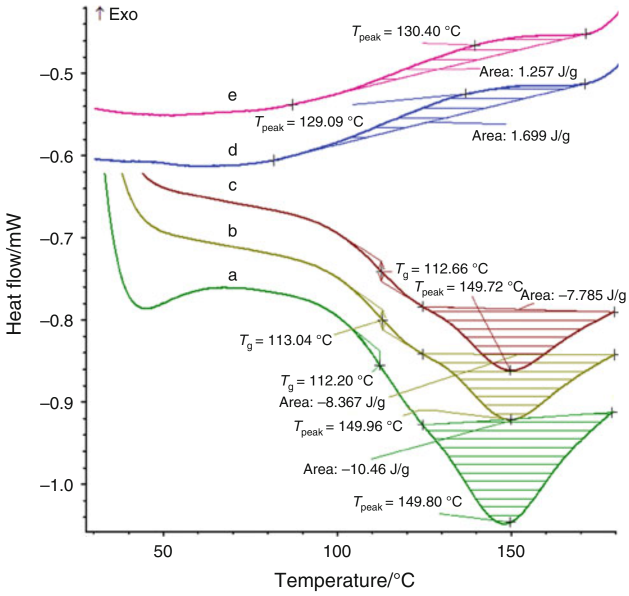

**Fig. 4** DSC curves of the sample PUSHDAN-2: *a* first heating curve, *b* second heating curve, *c* third heating curve, *d* first cooling curve and *e* second cooling curve

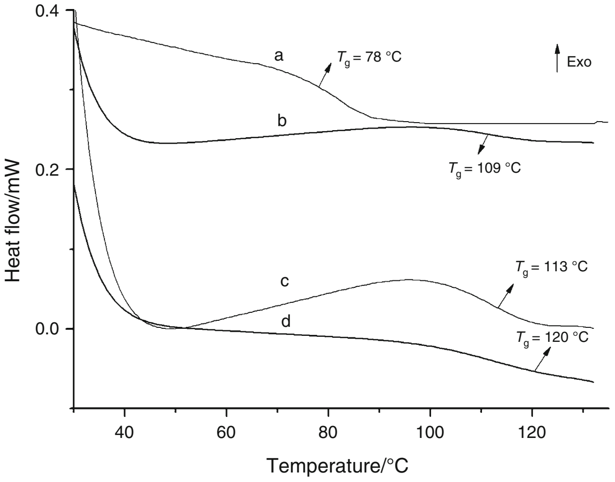

**Fig. 5** Effect of increasing silica content on $T_g$s: *a* BTESDAM, *b* PUSHDAN-1, *c* PUSHDAN-2, *d* PUSHDAN-3

formation of furan-maleimide adducts was accompanied by a decrease in the furan absorption intensity and a shift to lower wavenumber values of the carbonyl absorption band (from 1,714 to 1,710 cm$^{-1}$) [35]. The recovery reaction is not complete probably due to the rigidity of the dienic component (which now is a silica network with free furyl groups), which leads to the slowing down of the reaction. So, after heat treatment at 80 °C for 6 h, the carbonyl band shifts back to the initial value, while the furan absorption band decreases in intensity, indicating the complete reformation of the cycloadduct.

**Table 3** Heat capacities and related crosslinking data

| Sample code | Heat capacity, $C_p$/J g$^{-1}$ K$^{-1}$ | $\rho'_c$ |
|---|---|---|
| BTESDAM | 2.6386 | 0.0000 |
| PUSHDAN-1 | 2.5901 | 0.0184 |
| PUSHDAN-2 | 2.5777 | 0.0231 |
| PUSHDAN-3 | 2.4896 | 0.0565 |

## *DSC*

DSC analyses are often implied in characterizing materials with thermoreversible properties [36, 37]. Figure 4 indicates three heating cycles of the sample PUSHDAN-2 recorded in the temperature range from 30 to 180 °C and two cooling curves from 180 to 30 °C at a cooling rate of −5 °C/min with liquid nitrogen. A reproducible glass transition temperature ($T_g$) was observed at a value of 113 °C on all three heating curves corresponding to the $T_g$ of the crosslinked network. This transition underwent a broad endothermic process at a peak temperature value of 150 °C. A wider and less intense exothermic peak was observed on both cooling curves at a peak temperature value around 130 °C.

The endothermic process is attributed to the rDA reaction which mainly involves the chemical de-bonding between maleimide and furfuryl moieties in the crosslinked network structure [1, 38, 39]. On the cooling segments, the networks repolimerized via DA reaction. Process enthalpies yielded similar values of −10.46, −8.367, and −7.785 J g$^{-1}$ for rDA reaction and 1.699 and 1.257 J g$^{-1}$ for DA reaction, respectively.

Figure 5 displays the glass transition temperatures ($T_g$s) on the second heating curves of samples PUSHDAN-(1-3). The DSC curve for the non-crosslinked macromonomer adduct of a semi-solid glassy texture (BTESDAM) was also recorded until a $T_g$ was observed at 78 °C. $T_g$s shifted to slightly higher values with increasing silica content. The increase of silica content in the solution composition increased the crosslinking density from sample PUSHDAN-1 to PUSHDAN-3 due to weaker segmental motion of the chains. This lead to chain stiffness because of a reduction of free volume in the network [40, 41]. It has been also reported that silicone crosslinking groups enhance the toughness of the network as the Si–O bonds are known to be stronger compared to C–C bonds [42].

$C_p$s values and crosslinking density values are given in Table 3. It can be observed that crosslinking density values increase with the decrease of $C_p$s values, as expected. The $C_p$ is an energetic characteristic of the chain segments movement. Upon increasing values of the crosslinking degree, reduction of free volume between chain segments

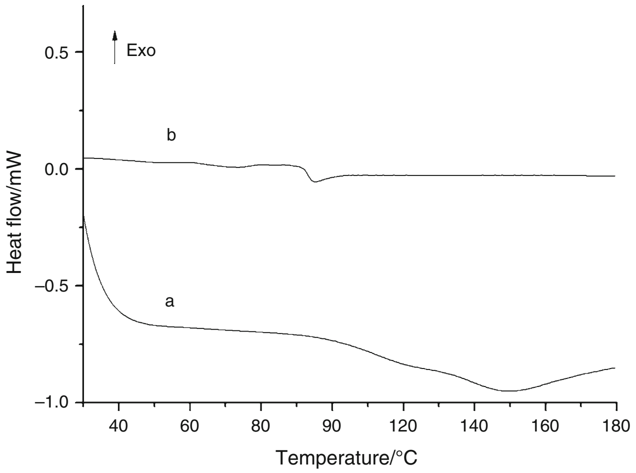

**Fig. 6** DSC curves of samples: *a* PUSHDAN-1 (second heating curve) and *b* PUSHDAM-1 (first heating curve)

sterically hinders their movement, thus lowering the $C_p s$ values.

A comparative DSC study was conducted between a sample obtained by DA polymerization (PUSHDAN-1) and another one through MA reaction [43] (PUSHDAM-1). Both samples were heated at a rate of 20 °C/min. Figure 6 displays the second heating curve of the sample PUSHDAN-1 (Fig. 6a) and the first heating curve of the sample PUSHDAM-1 (Fig. 6b). The sample obtained through MA reaction presented a single endothermic transition at a centered temperature value of 93 °C. Sample PUSHDAN-1 exhibited a $T_g$ at a 109 °C, as also shown in Fig. 5, and the wide endothermic peak characteristic for the rDA process at a temperature value of 150 °C, similar to PUSHDAN-2. This highlighted the capability of the latter system as a thermally remendable material.

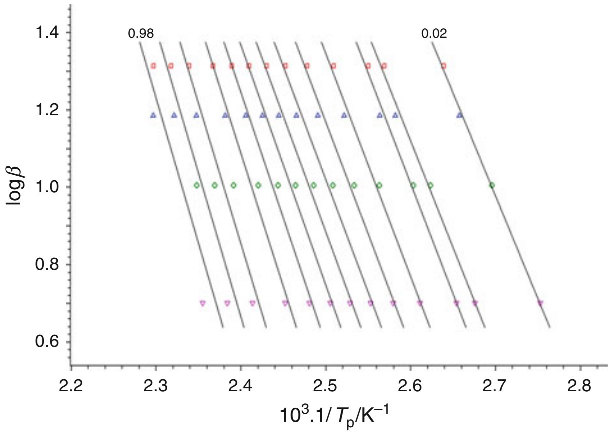

**Fig. 7** Plot of heating rate versus reciprocal absolute temperature

**Table 4** Global kinetic parameters determined by FWO method

| α | $E_a$/kJ mol$^{-1}$ | $A$/s |
|---|---|---|
| 0.02 | 95.83 ± 3.52 | $9.33 \times 10^9$ |
| 0.1 | 103.15 ± 6.25 | $1.162 \times 10^{11}$ |
| 0.2 | 104.18 ± 7.56 | $2.754 \times 10^{11}$ |
| 0.3 | 104.20 ± 8.43 | $2.951 \times 10^{11}$ |
| 0.4 | 105.37 ± 8.57 | $4.266 \times 10^{11}$ |
| 0.5 | 108.07 ± 8.19 | $9.772 \times 10^{11}$ |
| 0.6 | 112.05 ± 8.24 | $3.236 \times 10^{12}$ |
| 0.7 | 117.61 ± 9.56 | $1.659 \times 10^{13}$ |
| 0.8 | 124.78 ± 13.63 | $1.318 \times 10^{14}$ |
| 0.9 | 132.24 ± 24.29 | $10^{15}$ |
| 0.98 | 137.2 ± 47.57 | $3.09 \times 10^{15}$ |

## *Kinetic study*

The sum of all the basic steps of the rDA reaction equals the enthalpy change of the process. Owing to this aspect, the DSC data permit the evaluation of kinetic parameters of the reaction. Estimations can be both qualitative and semiquantitative. In a qualitative estimation, the position, shape, and number of DSC peaks are considered. In a semiquantitative estimation, the thermochemistry and the kinetics of the rDA reaction relate to the area and shape of the observed endothermic peak. The shape of the peak and the minimum and maximum peak temperatures are controlled by the kinetics, while the peak area is determined by the enthalpy change [44].

The different expressions of rate equations used in kinetic analysis of solid state reactions can be found in the literature [45]. Under non-isothermal conditions, examples of different shapes of the theoretic thermal analysis curves of the conversion degree (α), and alternatively, the rate of

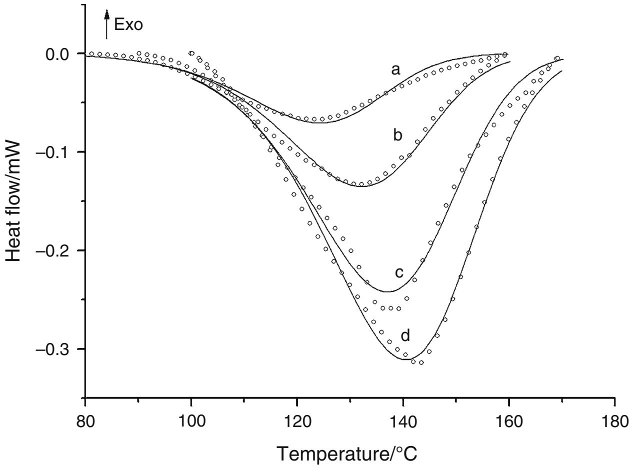

**Fig. 8** Comparison of experimental curves (*open circle*) with those calculated from kinetic data (*straight line*) at: *a* 5, *b* 10, *c* 15 and *d* 20 °C min$^{-1}$

change of $\alpha$, ($d\alpha/dT$), as functions of temperature, corresponding to the rate equations, can also be found in the literature [46]. These curves were constructed by means of the Doyle approximation [25] for the temperature integral.

The kinetic features of the reaction can only be estimated from a single dynamic (i.e., $\alpha$ and $T$) experiment if assumptions are made about the form of the rate expression. It is often assumed, without appropriate justification, that the reaction of interest can be regarded as a first order process, Eq. (6), where $f(\alpha)$ is the conversion function [46].

$$f(\alpha) = 1 - \alpha \tag{6}$$

The kinetic plot obtained by the FWO method and global process parameters values are given in Fig. 7 and Table 4. $E_a$ values for the rDA reaction vary from 95.83 to 137.2 kJ mol$^{-1}$. $E_a$ values increase with conversion degree thus suggesting that the process takes place in a successive reaction pattern [47]. Multivariate non-linear regression method was performed to determine reaction model for the four heating rates and to find the real form of the conversion function [47]. After testing of 16 reaction types, the best results were obtained for a $n$-th order reaction form, given in Eq. (7). A simple single step reaction model was found to be the best fit for the chosen kinetic pattern.

**Table 5** Kinetic parameters of the rDA reaction by multivariate non-linear regression method

| Heating rate, $v_h$/°C min$^{-1}$ | $E_a$/kJ mol$^{-1}$ | $A$/s | $n$ | $\Delta H$/J g$^{-1}$ |
|---|---|---|---|---|
| 5 | 112.21 | $3.92 \times 10^{12}$ | 1.24 | −32.26 |
| 10 | | | | −32.85 |
| 15 | | | | −27.64 |
| 20 | | | | −28.27 |

$$f(\alpha) = (1 - \alpha)^n \tag{7}$$

In order to check the form of the conversion function and the accuracy of the kinetic parameters, the experimental curves were compared to software simulated ones, by multivariate non-linear regression, using data presented in Table 4. Figure 8 shows the comparison of experimental data with simulated data. The value 0.995305 of the correlation coefficient indicated good fitting between experimental and calculated data. The correlation coefficient value very close to 1 proves the validity of the chosen kinetic model. The parameters of the rDA reaction obtained through multivariate non-linear regression method are given in Table 5.

It can be observed that the kinetic parameters corresponding to the rDA process and determined by multivariate non-linear regression method are in the range of global ones determined by FWO method. Moreover, $E_a$ and

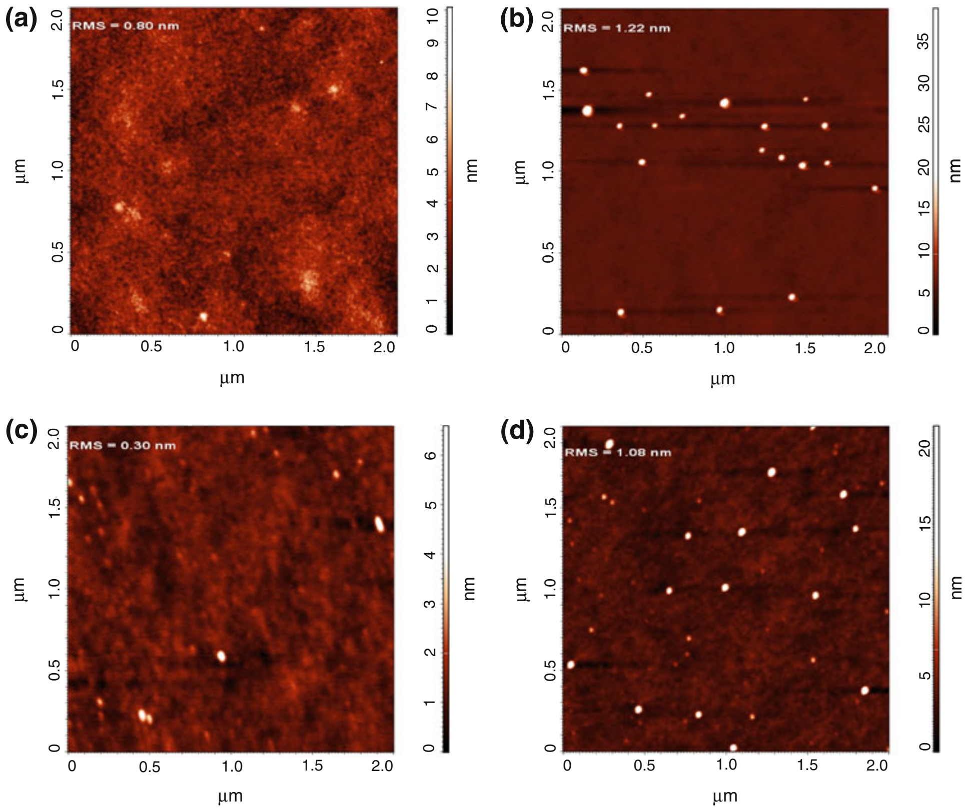

**Fig. 9** AFM images of: **a** PUSHMAN-1, **b** PUSHMAN-2, **c** PUSHDAN-1 and **d** PUSHDAN-3

$A$ values of 112.21 kJ mol$^{-1}$ and $3.92 \times 10^{12}$ (Table 5) are almost equivalent to those corresponding to an $\alpha$ value of 0.6. The main difference between the two applied kinetic methods is the form of the conversion function. If FWO method imposes a first order reaction model, multivariate non-linear regression method found the best kinetic fit between experimental and simulated data for an $n$-th order reaction model.

### *Morphological studies*

The morphology of the films PUSHMAN-1,2 and PUSHDAN-1,3 has been investigated by AFM technique (Fig. 9a–d). In general, the topographic features obtained with AFM for hybrid materials films were found to depend on the organic/inorganic phase behavior which also affects the values of mean squared roughness (RMS). RMS values depend on the surface textures since the surface roughness can be defined as the irregularities of the surface texture. The surfaces of PUSHMAN-1 and PUSHDAN-1 films, obtained by sol–gel process of BTESMAM and BTESDAM, respectively, without adding TEOS, have low roughness (RMS = 0.8 and 0.3 nm, respectively). The low values for roughness suggest that the prepared films have an excellent surface planarity. PUSHMAN-2 and PUSHDAN-3 films (obtained when adding TEOS) also have surfaces with low roughness (RMS = 1.22 and 1.08 nm, respectively). However, the roughness in this case is higher than in the case when TEOS is not used, suggesting that the degree of surface roughness when using TEOS is lower than in the hybrid materials obtained without adding TEOS. These results also suggest that the domain sizes of the inorganic phase are smaller in the hybrid materials obtained without adding TEOS [48].

Another observation that can be made is that the silica particles are more uniformly dispersed in the films of DA products than in the films of MA products, their size being comparable. The roughness of DA hybrid materials films is lower than that of MA hybrid materials films.

## Conclusions

New polyurethane and silica-based crosslinked networks were synthesized by both DA and MA reactions of BMI using FPTEOS or APTEOS, respectively, followed by sol–gel process of triethoxysilane groups and TEOS. $^1$H-NMR confirmed the formation of the soluble non-crosslinked starting macromonomers used in both synthesis paths. The formation of the crosslinked network structures was evidenced by ATR–FTIR method. ATR–FTIR, together with DSC method, was also used in demonstrating the thermally remendable character of the samples obtained through DA process. Both methods showed the reproducibility of the rDA reaction upon heating and that of the DA process upon cooling the samples. Heat capacities and crosslinking densities were determined by DSC technique. $T_g$s and crosslinking density values increased with silica amount increase and $C_p$s values decrease.

Global kinetic parameters were determined by FWO isoconversional method. A good correlation between experimental data and simulated data was found proving the accuracy of the chosen kinetic model.

Morphological studies, by AFM technique, indicated lower roughness and more uniformly dispersed silica particles in the DA obtained films.

**Acknowledgements** This study was supported by a grant of the Romanian National Authority for Scientific Research, CNCS–UEFISCDI, project number PN-II-ID-PCE-2011-3-0187.

## References

1. Teramoto N, Arai Y, Shibata M. Thermo-reversible Diels–Alder polymerization of difurfurylidene trehalose and bismaleimides. Carbohydr Polym. 2006;64:78–84.
2. Carlson HC, Goretta KC. Basic materials research programs at the US air force office of scientific research. Mater Sci Eng Part B. 2006;132:2–7.
3. Dry CM, Sottos NR. Passive smart self-repair in polymer matrix composite materials. Conference on recent advances in adaptive and sensory materials and their applications. Virginia: Technomic; 1992. p. 438–444.
4. Dry CM. Passive smart materials for sensing and actuation. J Intell Mater Sys Struct. 1993;4:420–5.
5. Schmets AJM, van der Zwaag S. Proceedings of the first international conference on self healing materials. In: Supplement to springer series in materials science. Noordwijk: Springer; 2007.
6. White SR, Sottos NR, Geubelle PH, Moore JS, Kessler MR, Sriram SR, Brown EN, Viswanathan S. Autonomic healing of polymer composites. Nature. 2001;409:794–7.
7. Endo T, Nagai D. A novel construction of ring-opening polymerization and chemical recycling system. Macromol Symp. 2005;226:79–86.
8. Sassw F, Emig G. Chemical recycling of polymers. Chem Eng Technol. 1998;21:777–89.
9. Chen X, Wudl F, Mal AK, Shen H, Nutt SR. New thermally remendable highly cross-linked polymeric materials. Macromolecules. 2003;36:1802–7.
10. Chino K, Ashiura M. Thermoreversible crosslinking rubber using supramolecular hydrogen bonding networks. Macromolecules. 2001;34:9201.
11. Gheneim R, Perez-Berumen C, Gandini A. Diels–Alder reactions with novel polymeric dienes and dienophiles: synthesis of reversibly cross-linked elastomers. Macromolecules. 2002;35:7246–53.
12. Liu YL, Chen YW. Thermally reversible cross-linked polyamides with high toughness and self-repairing ability from maleimide- and furan-functionalized aromatic polyamides. Macromol Chem Phys. 2007;208:224–32.
13. Brand T, Klapper M. Control of viscosity through reversible addition of telechelics via repetitive Diels–Alder reaction in bulk. Des Monomer Polym. 1999;2:287–309.
14. Diakoumakos CD, Mikroyannidis JA. Polyimides derived from Diels–Alder polymerization of furfuryl-substituted maleamic

acids or from the reaction of bismaleamic with bisfurfurylpyromellitamic acids. J Polym Sci Part A. 1992;30:2559–67.

15. Gandini A, Belgacem MN. Furan in polymer chemistry. Prog Polym Sci. 1997;22:1203–379.
16. Goiti E, Huglin MB, Rego JM. Some observations on the copolymerization of styrene with furfuryl methacrylate. Polymer. 2001;42:10187–93.
17. Kennedy JP, Carlson GM. Synthesis, characterization, and Diels–Alder extension of cyclopentadiene telechelic polyisobutylene. IV. $\alpha,\omega$-Di(3-cyclopentadienyl-propyldimethylsilyl)polyisobutylene. J Polym Sci Polym Chem Ed. 1983;21:3551–61.
18. Laita H, Boufi S, Gandini A. The application of the Diels–Alder reaction to polymers bearing furan moieties. 1. Reactions with maleimides. Eur Polym J. 1997;33:1203–11.
19. Mikroyannidis JA. Synthesis and Diels–Alder polymerization of furfurylidene and furfuryl-substituted maleamic acids. J Polym Sci Part A. 1992;30:125–32.
20. Gaina V, Ursache O, Gaina C, Buruiana E. Novel thermally-reversible epoxy-urethane networks. Des Monomer Polym. 2012; 15:63–73.
21. Vera-Graziano R, Hernandez-Sanchez F, Cauich-Rodriguez JV. Study of crosslinking density in polydimethylsiloxane networks by DSC. J Appl Polym Sci. 1995;55:1317–27.
22. Furukawa GT, Douglas TB, McCloskey RE, Ginnings DC. Thermal properties of aluminum oxide from 0 K to 1200 K. J Res Nat Bur Stand. 1956;57:67–82.
23. van Ekeren PJ. Thermodynamic background to thermal analysis and calorimetry. In: Brown ME, editor. Handbook of thermal analysis and calorimetry. Amsterdam: Elsevier; 1998. p. 90–1.
24. Haines PJ, Reading M, Wilburn FW. Differential thermal analysis and differential scanning calorimetry. In: Brown ME, editor. Handbook of thermal analysis and calorimetry. Amsterdam: Elsevier; 1998. p. 340–1.
25. Doyle CD. Estimating isothermal life from thermogravimetric data. J Appl Polym Sci. 1962;6:639–42.
26. Rabek JF, editor. In: Experimental methods in polymer chemistry. Chichester: Wiley; 1980. p. 241.
27. Hagiwara T, Suzuki I, Takeuchi K, Hamana H, Narita T. Synthesis and polymerization of *N*-(4-vinylphenyl)maleimide. Macromolecules. 1991;24:6856–8.
28. Wu W, Wang D, Wang P, Zhu P, Ye C. Thermally stable nonlinear optical polyimide functionalized by *N*,*N*-diallylamino-substituted chromophore. J Appl Polym Sci. 2000;77:2939–47.
29. Ozawa T. A new method of analysing thermogravimetric data. Bull Chem Soc Jpn. 1965;38:1881–6.
30. Opfermann J, Kaisersberger E. An advantageous variant of the Ozawa–Flynn–Wall analysis. Thermochim Acta. 1992;203: 167–75.
31. Hatakeyama T, Liu Z, editors. Handbook of thermal analysis. Chichester: Wiley; 1998. p. 47–8.
32. Hatakeyama T, Liu Z, editors. Handbook of thermal analysis. Chichester: Wiley; 1998. p. 359–60.
33. Tian Q, Rong MZ, Zhang MQ, Yuan YC. Optimization of thermal remendability of epoxy via blending. Polymer. 2010;51: 1779–85.
34. Yu YY, Chen CY, Chen WC. Synthesis and characterization of organic–inorganic hybrid thin films from poly(acrylic) and monodispersed colloidal silica. Polymer. 2003;44:593–601.
35. Kavitha AA, Singha NK. Smart “all acrylate” ABA triblock copolymer bearing reactive functionality via atom transfer radical polymerization (ATRP): demonstration of a “click reaction” in thermoreversible property. Macromolecules. 2010;43:3193–205.
36. Chen X, Dam MA, Ono K, Mal A, Shen H, Nutt SR, Sheran K, Wudl F. A thermally re-mendable cross-linked polymeric material. Science. 2002;295:1698–702.
37. Zhang Y, Broekhuis AA, Picchioni F. Thermally self-healing polymeric materials: the next step to recycling thermoset polymers? Macromolecules. 2009;42:1906–12.
38. Kavitha AA, Singha NK. Atom-transfer radical copolymerization of furfuryl methacrylate (FMA) and methyl methacrylate (MMA): a thermally-amendable copolymer. Macromol Chem Phys. 2007;208:2569–77.
39. Wouters M, Craenmehr E, Tempelaars K, Fischer H, Stroeks N, van Zanten J. Preparation and properties of a novel remendable coating concept. Prog Org Coat. 2009;64:156–62.
40. Srikant SK, Arjumand AK, Mrityunjaya IA, Mahadevappa YK. Synthesis and characterization of hybrid membranes using poly(vinyl alcohol) and tetraethylorthosilicate for the pervaporation separation of water–isopropanol mixtures. J App Polym Sci. 2004;94:1304–15.
41. Hsu YG, Lin FJ. Organic-inorganic composite materials from acrylonitrile–butadiene–styrene copolymers and silica through an in situ sol–gel process. J Appl Polym Sci. 2000;75:275–83.
42. Carraher CE Jr, Pittman CU Jr. Industrial polymers handbook. Weinheim: Wiley; 2001. p. 1284.
43. Jothibasu S, Kumar AA, Alagar M. Synthesis of maleimide substituted polystyrene–silica hybrid utilizing Michael addition reaction. J Sol Gel Sci Technol. 2007;4:337–45.
44. Pawelec B, Fierro JLG. Applications of thermal analysis in the preparation of catalysts and in catalysis. In: Brown ME, Gallagher PK, editors. Handbook of thermal analysis and calorimetry. Amsterdam: Elsevier; 2003. p. 178.
45. Galwey AK, Brown ME. Kinetic background to thermal analysis and calorimetry. In: Brown ME, editor. Handbook of thermal analysis and calorimetry. Amsterdam: Elsevier; 1998. p. 169–71.
46. Galwey AK, Brown ME. Kinetic background to thermal analysis and calorimetry. In: Brown ME, editor. Handbook of thermal analysis and calorimetry. Amsterdam: Elsevier; 1998. p. 190–4.
47. Opferman J. Kinetic analysis using multivariate non-linear regression. J Therm Anal Calorim. 2000;60:641–58.
48. Wahab MA, Kim I, Ha CS. Microstructure and properties of 3,3′,4,4′-biphenyltetracarboxylic dianhydride (BPDA)-*p*-phenylene diamine (PDA) polyimide/poly(vinylsilsesquioxane) hybrid nanocomposite films. J Polym Sci Part A. 2004;42:5189–519.